doi:10.1016/j.jmb.2010.09.047 J. Mol. Biol. (2010) 404, 439–455

Contents lists available at www.sciencedirect.com

Journal of Molecular Biology

journal homepage: http://ees.elsevier.com.jmb

Coupling Translocation with Nucleic Acid Unwinding by NS3 Helicase

Jin Yu[1]*, Wei Cheng[2], Carlos Bustamante[1,3,4,5] and George Oster[4,6]*

[1]Department of Physics, University of California, Berkeley, CA 94720, USA
[2]Department of Pharmaceutical Science, University of Michigan, Ann Arbor, MI 48109, USA
[3]Department of Chemistry, University of California, Berkeley, CA 94720, USA
[4]Department of Molecular and Cell Biology, University of California, Berkeley, CA 94720, USA
[5]Howard Hughes Medical Institute, University of California, Berkeley, CA 94720, USA
[6]Department of Environmental Science, Policy and Management, University of California, Berkeley, CA 94720, USA

Received 23 June 2010;
received in revised form
27 August 2010;
accepted 20 September 2010
Available online
29 September 2010

Edited by A. Pyle

Keywords:
molecular motor;
helicase;
DNA/RNA unwinding;
diffusion;
stochastic simulation

We present a semiquantitative model for translocation and unwinding activities of monomeric nonstructural protein 3 (NS3) helicase. The model is based on structural, biochemical, and single-molecule measurements. The model predicts that the NS3 helicase actively unwinds duplex by reducing more than 50% the free energy that stabilizes base pairing/stacking. The unwinding activity slows the movement of the helicase in a sequence-dependent manner, lowering the average unwinding efficiency to less than 1 bp per ATP cycle. When bound with ATP, the NS3 helicase can display significant translocational diffusion. This increases displacement fluctuations of the helicase, decreases the average unwinding efficiency, and enhances the sequence dependence. Also, interactions between the helicase and the duplex stabilize the helicase at the junction, facilitating the helicase's unwinding activity while preventing it from dissociating. In the presence of translocational diffusion during active unwinding, the dissociation rate of the helicase also exhibits sequence dependence. Based on unwinding velocity fluctuations measured from single-molecule experiments, we estimate the diffusion rate to be on the order of 10 s^{-1}. The generic features of coupling single-stranded nucleic acid translocation with duplex unwinding presented in this work may apply generally to a class of helicases.

Introduction

Helicases are enzymes essential for every aspect of DNA or RNA metabolism.[1–3] Like most motor proteins, helicases use the free energy from NTP hydrolysis to translocate along single-stranded (ss) DNA or RNA, unwind double-stranded (ds) duplex, or displace proteins along the nucleic acid track.[4,5] There are six helicase superfamilies classified according to their signature sequence motifs.[1,6] Among them, the helicase superfamily 1 and 2 (SF1 and SF2) are the two largest groups, consisting mainly of monomeric and dimeric helicases,[7] with each monomer being a single polypeptide chain containing two RecA-like folds.[8,9] Other families of helicases often assemble in multimeric forms, such as hexamers.[3,10,11]

Hepatitis C is a disease that affects about 180 million people worldwide. The C-terminal portion of nonstructural protein 3 (NS3) from the hepatitis C virus (HCV) forms a three-domain enzyme and is classified as an SF2 helicase,[2,12] while the N-terminal

*Corresponding authors. 216 Wellman Hall, University of California, Berkeley, CA 94720, USA. E-mail addresses: jinyu@berkeley.edu; goster@berkeley.edu.

Abbreviations used: NS3, nonstructural protein 3; ss, single-stranded; ds, double-stranded; SF, superfamily; HCV, hepatitis C virus.

portion of the NS3 forms a protease domain. The nonstructural proteins are responsible for replication and packaging of the viral genome. The helicase portion of NS3 is the first crystallized HCV protein known to hydrolyze ATP and to unwind DNA or RNA;[13–15] its exact role in viral replication is unclear, although essential. Identifying inhibitors that target the NS3 helicase would help resolve the functional issue and possibly develop anti-HCV drugs.[16] In its monomeric form, the NS3 helicase can translocate along ss nucleic acids in the 3′ to 5′ direction,[17–22] unwind duplex regions, and displace other bound proteins on the nucleic acid.[23] The helicase shares with other monomeric translocases the two RecA-like domains (1 and 2),[7] with an ATP binding site located in between the two domains. Figure 1 shows

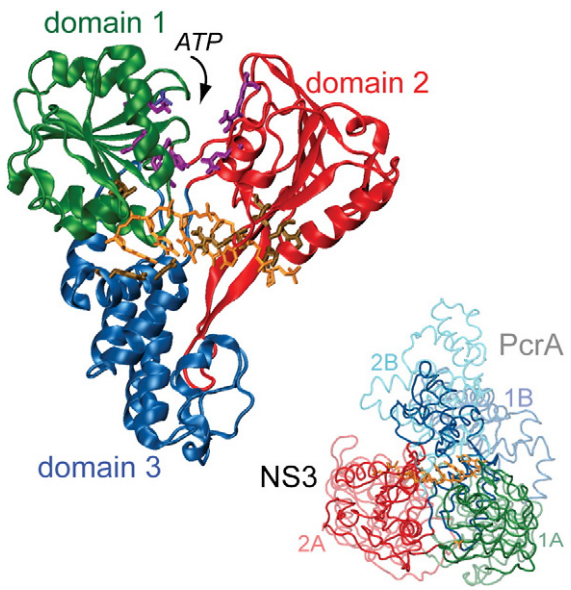

Fig. 1. The structure of HCV-NS3 helicase and its structural alignment with PcrA in two translocase domains. (Left) The NS3 helicase domain with a bound oligonucleotide obtained from a high-resolution structure (Protein Data Bank ID: 1A1V).[14] Domains 1, 2, and 3 of NS3 are in green, red, and blue, respectively. The poly(dU) oligonucleotide was crystallized with six residues visible, in orange. The ATP binding site is located in between domains 1 and 2, with residues essential for ATP binding and hydrolysis in purple (these include K210, D290, E291, and H293 from domain 1 and Q460 and R467 from domain 2). The oligonucleotide threads through NS3 in between domain 3 and the other two domains, with important residues that interact with the oligonucleotide in brown (from left to right, they include W510, T269, E493, R393, T411, T450, and H369).[12] (Right) Structural alignment[24] between the two translocase domains of the NS3 helicase and that of the PcrA helicase.[25,26] The PcrA helicase is shown in semi-transparent representation, with domains colored the same as their corresponding domains in the NS3 helicase: 1A to domain 1 (green), 2A to domain 2 (red), 1B (2B) to domain 3 (blue). The molecular images were generated by VMD.[27]

the NS3 helicase in complex with a 6-nt piece of ssDNA obtained from previous high-resolution structural studies.[14] Essential residues involved in ATP and ssDNA binding are also depicted. The ssDNA threads through a groove between domain 3 and the two translocase domains (1 and 2) of the enzyme. In the lower right portion of Fig. 1, a structural alignment is shown between domains 1 and 2 of the NS3 helicase and the two RecA-like domains 1A and 2A of an SF1 helicase PcrA.[25,26] According to the alignment algorithm,[24,28] the overall PcrA structure is not very similar to that of the NS3 helicase; however, the two translocase domains in these two helicases are structurally similar.

Recently, high-resolution structures of the NS3 helicase have been obtained bound with ATP analogs.[29] These structures provide conformational snapshots suggesting that two nucleic acid binding surfaces (NABS2 and NABS1), located on domains 1 and 2, respectively, are required for the helicase to move unidirectionally along the ss.[29] Upon ATP binding between the two translocase domains and release of hydrolysis products (ADP and P_i), the two binding sites alternate moving forward 1 nt at a time. The movements are coordinated through intra- and interdomain motions. Overall, the motor walks along the ss in an 'inchworm' fashion. This movement is similar to that proposed for the SF1 PcrA helicase,[25,30] although the exact domain movements and detailed structural characteristics differ somewhat.

PcrA and monomeric Rep and UvrD[1,7] are among the best studied SF1 helicases. ATP also binds into the cleft between the two RecA-like translocase domains (1A and 2A) of PcrA. As in NS3, the cleft 'closes' as ATP binds and 'opens' upon release of the hydrolysis products.[25,29] According to structural analyses and simulation studies,[25,30,31] the unidirectional movement of the PcrA helicase along ssDNA is achieved by coordinating the ATP hydrolysis cycle with individual translocase domain motions. In addition, PcrA domain 1B (and/or part of 2B) corresponds to domain 3 in NS3 (see Fig. 1). Based on crystal structure, it appears that domain 2B may destabilize the duplex DNA via conformational coupling to the ATP binding region in PcrA[25] [see Fig. S1 from Supporting Information (SI)]; however, the exact role of this domain remains controversial as deletion of the entire 2B domain in Rep results in a fully functional monomeric helicase.[32] In this work, we assume that the NS3 helicase shares important features with PcrA in its ss translocation activity; that is, the helicase coordinates movements of domains 1 and 2 with the ATP hydrolysis cycles such that each domain steps forward 1 nt at a time. The unidirectional translocation model we develop for the NS3 helicase is, therefore, based mainly on computational work on PcrA.[30,31]

Recent measurements on the ss translocation activity of NS3[20–22] show that the translocation can be affected by sugar and base moieties of the ss such that the helicase translocates faster on ssRNA than on ssDNA.[22] Nevertheless, structural studies have shown that the helicase interacts with the ss dominantly via backbone interactions.[14,25,29–31] Thus, the base effect on the translocation, if any, is likely indirect, arising from base–backbone couplings in the ss. In this work, we assume that the ss translocation of the helicase is sequence independent as suggested for PcrA,[25,30,31] and regard the backbone–base coupling as a higher-order effect.

Previous biochemical measurements on NS3 helicase also show that its binding affinity to ssDNA is significantly lowered when the helicase is bound with ATP (or an analog).[33] Moreover, the helicase appears to unwind base pairs at the junction simply by binding to the duplex.[34] These results suggest that the NS3 helicase unwinding/translocation is coupled with its Brownian fluctuations as follows:[33,34] ATP binding loosens the grip of the helicase on the ss so that the helicase may transiently move randomly and bidirectionally (i.e., diffuse) along the ss; ATP hydrolysis and product release re-induce tight binding of the helicase to the nucleic acid, resulting in a biased forward movement of 1 nt that leads to directional translocation[33] and duplex unwinding.[34] However, the structural basis and the molecular mechanism of the directional movement of the NS3 helicase have remained unclear.

Here, we model the translocation and unwinding activities of NS3 helicase by combining its structural[14,29] and biochemical properties.[33,34] For the directional movement of the helicase, we adopt an alternating domain stepping model similar to that used for PcrA,[30,31] consistent with the structural studies of NS3.[14,29] In addition, we included in our model the diffusive property of NS3 helicase as suggested from Ref. 34. This means that the helicase can diffuse or hop forward and backward along the ss when it is bound with ATP. Thus, our model combines the inchworm-like directional stepping feature[25,30] with nontrivial Brownian diffusion.[34]

In modeling NS3 unwinding activity, we have incorporated properties of T7 helicase unwinding[35,36] that seem to apply to NS3. Studies suggested that the unwinding of the T7 helicase is not associated with dTTP binding but with hydrolysis or products release.[36] We assume in this work that binding of ATP induces only the closing of the two domains promoting the stepping of domain 1 (the trailing domain of the enzyme) forward by 1 nt. Upon hydrolysis and release of products, the two translocase domains must separate again. This separation is achieved by the stepping forward of domain 2 (the leading domain) by 1 nt. This promotes the unwinding of the duplex at the fork and completes the mechanochemical cycle of the motor. Recent experiments supported this assumption and suggested that P_i release triggers the power stroke for NS3 unwinding.[37]

The unwinding and translocation model proposed here incorporates many more structural and biochemical properties of the motor than previous studies.[38–40] Importantly, the sequence effect of helicase unwinding has not been addressed previously but is explicitly modeled in this work. To calibrate and quantify the current model, we have fitted our numerical results with experimental data on RNA unwinding of NS3 from single-molecule optical tweezer measurements.[18,41]

However, there are additional structural and mechanistic features of NS3 that we have not explicitly taken into account in the current model, which are likely related to the protease domain of the full-length NS3. In addition to the ss nucleic acid binding sites revealed from the crystal structure,[14] single-molecule fluorescence resonance energy transfer experiments[42] and structural-based modeling[13,43] suggest that there are also secondary RNA binding sites in NS3. Moreover, the protease domain in NS3 plays an important role in RNA helicase activity and greatly facilitates binding of substrate RNA by NS3.[44] Although these features have not been explicitly considered here, it is possible that the enzyme contacts the dsRNA region upstream of the junction through its protease and/or its domain 3. These contacts anchor the enzyme on the ds region, destabilizing the fork and permitting the translocase domains to open the fork. Such a scenario is not inconsistent with the detailed mechanism described here and may explain the 11-bp step size observed in single-molecule optical tweezers[18] and bulk kinetic experiments.[43]

In the following, we first describe how we constructed the model and then show how several experimental observations can be understood in terms of the model.

Results

Constructing the model

In this part, we describe how we model the translocation of the NS3 helicase along ssDNA or ssRNA and how it subsequently unwinds the RNA/DNA duplex when it encounters a fork. We assume qualitatively that the NS3 helicase behaves the same on the DNA and RNA, although the magnitudes of the activities may differ.

Translocation along the ss nucleic acid

Previous biochemical measurements suggest that NS3 helicase translocates along the ss nucleic acid in

two alternating states: (a) a high-affinity state as the motor binds tightly to the ss when the ATP binding site is empty (so-called 'apo' state) and (b) a low-affinity state as the motor loosely binds to the ss when the catalytic site is occupied by ATP.[33] Henceforth: 'a' refers to the *a*po state, and 'b' refers the ATP-*b*ound state. In each state, in principle, the helicase (domains 1, 2, and 3 together) can move back and forth by 1 nt along ss. The movements are characterized by a forward rate, r_i^+, and a backward rate, r_i^- (i=a, b). The motor has no directional bias within each state—the directionality arises from transitions between the states via ATP hydrolysis cycles. Therefore, we denote $r_a^+ = r_a^- = r_a$ and $r_b^+ = r_b^- = r_b$. To be consistent with the motor–ss affinities, we require $r_a < r_b$, so that high (low) ss affinity corresponds to low (high) translocation mobility.[30] Since NS3 helicase binds the ss tightly in the apo state, we let $r_a \to 0$, while maintaining $r_b > 0$. That is, the low affinity of the motor to the ss in the ATP state allows it to move randomly and birectionally (diffuse) as suggested from experimental work.[33,34] Though direct observation on the helicase diffusion has not been made, the diffusive character is realistic as long as the diffusion happens faster than dissociation of the helicase from the ss; that is, r_b is larger than the dissociation rate k_{off}^b in the ATP-bound state. Later, we will show that this is indeed true for our NS3 model ($r_b \sim 10\ s^{-1}$ and $k_{off}^b \sim 1.7\ s^{-1}$).

The high and low motor–ss affinities are also supported by structural studies showing that the low motor–ss affinity upon ATP binding is due to structural rearrangements that lose several hydrogen-bond interactions between the NS3 helicase and the 3′ ssDNA segments.[29] Similar observations have been reinforced by computational studies on PcrA showing that hydrogen-bonding interactions between the helicase and the 3′ ssDNA segment are weaker in the ATP-bound state than in the apo state.[31]

Alternating domain stepping for directionality

Like the PcrA helicase, monomeric NS3 helicase can be regarded as a two-domain translocase[23] (see Fig. 1). We have assumed, therefore, that the translocation mechanisms are similar for these two helicases. In particular, in both helicases, the two translocase domains are relatively separated from each other in the absence of ATP, but move closer together when ATP binds in between, and resume their original separation after hydrolysis products are released. We show below that this cycle of displacements causes the two domains to alternate moving forward 1 nt at a time as the helicase transits between the two states a and b. These properties are supported from structural studies of both helicases.[14,25,29]

In Fig. 2a, we illustrate the helicase translocation cycle of NS3. In this scheme, domain 1 (trailing/rear) and domain 2 (leading/front) each moves along the ss nucleic acid subject to their own potential of mean force whose period is 1 nt: green for domain 1 and red for domain 2. We denote by x_1, x_2 the location of the rear and front domain, respectively, along the ss. The position of the helicase as a whole is defined as the average position of the two domains, denoted by $x = (x_1 + x_2)/2$, and indexed by j (state a) or $j + 1/2$ (state b) located at the potential minima. The two domains are coupled to each other by a linear spring whose rest length is different in the two states. Before ATP binds, the motor is in state a at position j (configuration 1), and the rest length of the spring is l_0. In this configuration, both domains bind tightly to the ss via their individual potentials. Both potential barriers are high, but domain 1 sees a lower-energy barrier than domain 2. This property persists as ATP initially binds between the two domains (configuration 2) and the spring length shrinks from l_0 to $l_0 - 1$. Because of its lower-energy barrier, domain 1 hops forward faster than domain 2 hops backward. This leads to a stabilized ATP-bound configuration 3, with the motor in state b at the position $j + 1/2$, and the spring length equilibrated at $l_0 - 1$. The transition a → b (configuration 1 → 3) is assumed to be rate limited by ATP binding (rate $\omega_{ab}^I = k_{ET} \cdot [ATP]$). This is because both domain potential barriers decrease during the ATP binding process (i.e., ss affinity decreases as ATP binds), and the coupling spring can pull the individual domains together (configuration 2) strongly enough such that the domain 1 movement occurs very fast.

The low affinity of the NS3 helicase to the ss as ATP stably binds (configuration 3) allows the helicase to diffuse forward and backward along ss in state b. Essential conformation changes may take place upon stable ATP binding, so that the relative mobilities of the two domains can switch and domain 2 becomes more mobile than domain 1. Upon ATP hydrolysis and product (P_i and ADP) release (configuration 4), the two domains are driven apart as the coupling spring expands to its original rest length l_0. During this recoil power stroke, domain 2's lower barrier allows it to move forward 1 nt as the motor relaxes back to its apo state at configuration 5. Thus, the helicase has advanced forward 1 nt from from 1. The rate-limiting event during the transition b → a (configuration 3 → 5) is assumed to be domain 2's movement, which is coupled with product release (at rate $\omega_{ba}^{II} = k_{cat}$).[37] The rate-limiting domain movement is affected by the spring force. The spring force is relatively weak compared with the domain potentials (configuration 4; compare 2 and 4), which grow as the motor–ss affinity increases toward the apo state. Note that the rate-limiting steps were also arranged to be compatible with the unwinding properties assumed for the NS3 helicase. That is, the unwinding force is generated upon product release (i.e., the transition b → a is rate limited mechanically)

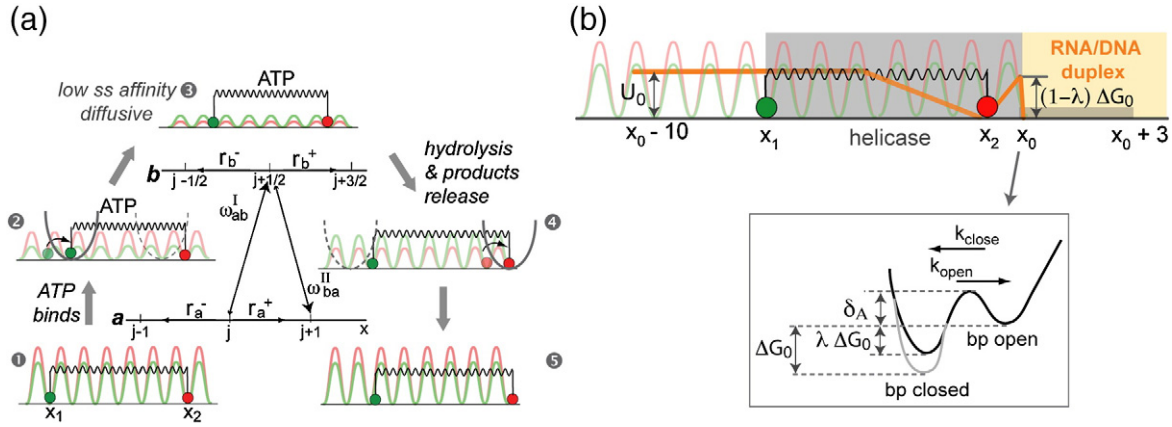

Fig. 2. The translocation and unwinding scheme of the NS3 helicase. (a) The ss translocation is modeled as a two-state process, based on the PcrA model.[30] State a is the apo state with the catalytic site empty. In state a, NS3 has a high affinity to the ssDNA/RNA. State b is the ATP-bound state. In state b, NS3 has a low affinity to the ss[33] and can hop (diffuse) to adjacent sites at rate r_b. The red disk represents front/leading domain 2 (at position x_2), and the green one represents rear/trailing domain 1 (at position x_1). The individual domain potentials along the ss are shown in the corresponding color.[30] Upon ATP binding (at rate ω^{I}_{ab}; configuration 1 to 2), the two domains are drawn closer to each other in comparison with the apo state; domain 1 steps forward 1 nt as it faces a lower potential barrier than domain 2. After ATP stably binds (configuration 3), domain 2 experiences a lower potential barrier than domain 1, such that upon hydrolysis product release, domain 2 steps forward 1 nt (at rate ω^{II}_{ba}; configuration 3 to 4) as the two domains separate from each other. In this way, the helicase translocates forward 1 nt over an ATP hydrolysis cycle (compare 5 to 1). (b) The schematics of NS3 helicase duplex unwinding. Shown are a binding configuration of the apo NS3 helicase at the ds–ss junction/fork, the individual domain potentials in the ss translocation [as in (a)], and effective potentials due to the presence of the duplex. In this helicase binding configuration, the duplex end is located at x_0, the front domain 2 is labeled at $x_2 = x_0 - 1$, and the rear domain 1 at $x_1 = x_0 - 7$. The bulk of the NS3 helicase (gray) covers a 7-nt ss tail region of the junction. Additionally, the front edge of the helicase (some region on domain 2 or 3) extends into the duplex backbone region for 3 nt. The base-pair-unwinding potential is located between $x_0 - 1$ and x_0 to prevent domain 2 from moving forward. The potential is resulted from helicase active unwinding, which reduces the base pair stabilization free energy from ΔG_0 to $\lambda \Delta G_0$ ($0 \le \lambda \le 1$) by supplying energy $(1-\lambda)\Delta G_0$. δ_A is the activation energy separating the base pair open to the closed state. The junction-stabilizing potential, depicted relative to domain 2 in this diagram, has its minimum located at current position $x_2 = x_0 - 1$, reaching a high plateau U_0 at 3 nt further, preventing the helicase from moving away from the junction. This potential likely results from the helicase front edge associating favorably with the duplex backbone for 3 nt. The association facilitates active unwinding and prevents the helicase from dissociating.

but not upon ATP binding (i.e., the transition a → b is chemically rate limited).[36,37] The exact details of the mechanochemical cycle of NS3 helicase translocation need to be elucidated in future experiments.

Unwinding duplex nucleic acid

Figure 2b shows the binding configuration of the NS3 helicase to the RNA/DNA junction when it abuts a duplex junction. In this configuration, the end base pair of the duplex at the junction is located at x_0 and the helicase covers the ss tail region of the junction for 7 nt, with its front domain 2 (red) labeled at $x_2 = x_0 - 1$ and the rear domain 1 (green) at $x_1 = x_0 - 7$. The 'front edge' of the helicase (from domain 2 and/or domain 3) extends into the duplex (backbone) region for an extra 3 nt. The 7-nt ss distance covered by the helicase was chosen to be consistent with its structure[14] (see the 6-nt oligonucleotide in between domains 1 and 2 in Fig. 1) and biochemical properties. Experimentally, the helicase binds to the junction and unwinds the duplex when the 3′ ss tail linked to the duplex is less than 7 nt long.[34] The extra 3 nt represents the backbone region of the duplex that is closely associated with the helicase front domain 2 and/or domain 3. The association stabilizes the helicase at the junction (discussed below) and, during each ATP cycle, facilitates base pair unwinding through backbone distortions, likely similar to PcrA (see Fig. S1). The overall 10-nt distance of the helicase, projected onto the nucleic acid track, is consistent with experimental measurements showing that the helicase binds to a DNA junction with a 10-nt ss tail as fast as it binds to a pure ssDNA of 10 nt long.[34] Detailed analyses are provided in the SI and Fig. S2.

Duplex effects during unwinding

The basic feature of duplex unwinding in the current model is that, as the helicase translocates along ss, it interacts with the RNA/DNA duplex at the junction where the base pairing/stacking blocks its progress. The hydrogen-bonded base pairing,

however, fluctuates between 'open' and 'closed', biased toward the closed state at equilibrium. This assumption about the base pair 'open↔close' equilibrium is reasonable since its fluctuation frequency (10^5–10^7 s^{-1})[38,45] is much faster than the helicase moving rate (10–10^2 s^{-1}). The energy of ATP hydrolysis driving ss translocation can also allow the helicase to actively 'tilt' the potential so that the base pair equilibrium is biased away from the closed state and toward the open state. The work to accomplish this is provided by exerting force on the hydrogen bonds of the base pair via the front domain movement and possibly also by perturbing the duplex structure with associated domain 2 and/or domain 3. Otherwise, the helicase would need to wait passively for transient spontaneous base pair opening to move forward,[46] which also requires that the helicase does not dissociate from the junction too fast. Additionally, the NS3 helicase can be stabilized at the junction (see SI text and Fig. S2). This stabilization has been demonstrated experimentally since the NS3 helicase shows a higher affinity to a duplex substrate with a 3′-ss tail than to a pure ss substrate of the same tail length (of 7 to 10 nt ss).[34] The stabilization can be achieved via helicase interactions with the duplex that also facilitate unwinding. Moreover, the stabilization can prevent the helicase from dissociating from the junction before unwinding proceeds.

Effective potentials of unwinding

To model the above effects during unwinding, we introduce two effective potentials at the junction along the helicase translocation coordinate x (see Fig. 2b) while keeping the same translocation potentials for domains 1 and 2 (as in Fig. 2a). Both unwinding potentials are shown as acting at the position of domain 2, and the corresponding energy minimum is located at $x_2 = x_0 - 1$ where domain 2 is labeled in Fig. 2b.

Base-pair-unwinding potential. The base-pair-unwinding potential is located between $x_0 - 1$ and x_0 when the NS3 helicase actively unwinds the duplex at its front domains (2 and 3). This potential tilts the open↔close equilibrium of the end base pair away from the closed state and toward the open state. Suppose the original free-energy difference between the base pair open and closed state, that is, the base pair stabilization free energy, is $\Delta G_0 \equiv G_{open} - G_{close} \geq 0$, so that the ratio between the base pair opening rate (k^0_{open}) and the closing rate (k^0_{close}) is $k^0_{open}/k^0_{close} = e^{-\Delta G_0}$. The helicase activity somehow decreases the base pair stabilization free energy from ΔG_0 to $\lambda \cdot \Delta G_0$ where $0 \leq \lambda \leq 1$ ($\lambda = 0$ corresponds to the maximum active case and $\lambda = 1$ corresponds to the minimum active or passive case). Here, we use λ as a phenomenological parameter to measure how active a helicase is during its unwinding activity. Note that the energy reduction in the base pair stabilization free energy occurs when the helicase supplies free energy $\varepsilon_{int} = (1-\lambda)\cdot\Delta G_0$ to the base pair. To model the interaction, we used a one-step linear potential, which is a special case of more general interaction potentials discussed in Ref. 38. As a result of this interaction, the ratio between the opening and closing rate of the end base pair changes to:

$$\frac{k_{open}}{k_{close}} = \frac{k^0_{open}}{k^0_{close}} e^{\varepsilon_{int}} = \frac{k^0_{open}}{k^0_{close}} e^{(1-\lambda)\cdot\Delta G_0} = e^{-\lambda\cdot\Delta G_0} \quad (1)$$

On the other hand, the forward movement rate (k_+) of the helicase at the position just before the potential, as well as the backward movement rate (k_-) just after, also changes from their original values ($k^0_\pm$) such that

$$\frac{k_+}{k_-} = \frac{k^0_+}{k^0_-} e^{-\varepsilon_{int}} = \frac{k^0_+}{k^0_-} e^{-(1-\lambda)\cdot\Delta G_0} \quad (2)$$

Here, the forward rate applies specifically to the 'catalytic' transition rate from b to a (k_{cat}) that couples with helicase domain 2 movement at $x_2 = x_0 - 1$, or to the forward diffusion rate (r_b^+) of the helicase bound with ATP. The backward rate applies to the backward diffusion rate (r_b^-) as the helicase domain 2 moves onto the duplex end at $x_2 = x_0$. To specify how much the forward and backward rates are individually affected, we used a factor $0 < \xi < 1$, such that $k_+ = k^0_+ e^{-\xi(1-\lambda)\Delta G_0}$ and $k_- = k^0_- e^{(1-\xi)(1-\lambda)\Delta G_0}$; this ensures the detailed balance condition in Eq. (2).

Notice that in the passive unwinding case suggested in Ref. 46, the helicase waits for spontaneous base pair opening to move forward without affecting the equilibrium. That is, when $\lambda = 1$, the base-pair-unwinding potential vanishes, and the forward and backward rates of the helicase are not affected via the potential. Indeed, we consider passive unwinding as an extreme case when $\lambda = 1$ (minimal active unwinding). Although the open–closed equilibrium of the end base pair is not affected when $\lambda = 1$, the model allows an extra probability of base pair opening if the helicase has an additional energy $\lambda \cdot \Delta G_0 + \delta_A$ that immediately activates a 'forced' closed→open transition (see Fig. 2b). Note that δ_A ranges about 0–10 k_BT (see SI on parameter tuning and Table S1). The extra probability is detectable if $\delta_A \to 0$. While $\delta_A \to 10$ k_BT, the extra probability approaches zero and the minimal active unwinding converges to the passive unwinding.

Junction-stabilizing potential. The junction-stabilizing potential comes from attractive interactions between the front edge of the helicase and the duplex (see Fig. 2b). The depth of this attractive potential is

denoted $U_0>0$. The attraction likely arises from helicase front edge interacting with the backbone of the duplex, similar to that observed in PcrA (see SI and Fig. S1). Interestingly, recent experimental studies indicate that bases immediately adjacent to the junction are less stacked than ssDNA bases elsewhere.[47] Hence, it is also possible that the partial unstacking of the bases at the junction contributes to the preferential helicase–duplex association.

As shown in Fig. 2b, the potential reaches a high plateau of U_0 when x_2 moves to x_0-4 or when the rear end (on domain 1) of the helicase in the apo state is 10 bp away from the duplex end ($x_1=x_0-10$) on the ss. As mentioned above, it has been measured that the NS3 helicase binds to the duplex DNA with a 10-nt ss tail as fast as it binds to a 10-nt ssDNA,[34] while the binding rate to the duplex with an ss tail of less than 10 nt (≥ 7 nt) is larger than that to the ss substrate of the same tail length. That is, when the rear end of the NS3 helicase is within 10 nt from the duplex end, the helicase can sense the duplex through its front-edge association with the duplex; when the rear end is at or beyond 10 nt, the duplex has no effect on the helicase.

Furthermore, the NS3 helicase has a higher affinity for the duplex with an ss tail than to the pure ss substrate of the same ss length (7–10 nt).[34] Thus, the magnitude of U_0 can be estimated from the measured affinities (see SI). Note that U_0 varies between the apo and the ATP-bound state as the helicase–duplex interactions switch between the two states (cf. structures of PcrA–DNA complexes in Fig. S1). We denote the junction stabilizing strength associated with these two states by U_o^a and U_o^b accordingly.

Another characteristic of this stabilizing potential is that it deepens along the translocation coordinate as the helicase approaches the junction. The potential energy along the strand is minimum when the front edge of the helicase extends into the duplex backbone region for 3 nt. At this energy minimum configuration (in the apo state), $x_2=x_0-1$, and correspondingly, the rear part of the helicase reaches 7 bp distance from the duplex end at $x_2=x_0-7$. As implied in the experiments,[34] a shorter distance than 7 nt between the helicase rear end and the duplex results in base pair unwinding. Overall, the junction-stabilizing potential is made consistent with the binding configuration of the NS3 helicase at the junction (see also Fig. S2). In general, the backward and forward rates of the helicase would also be affected by this potential. By specifying a factor $0<\zeta<1$ similar to ξ for the base-pair-unwinding potential, the backward rates are decreased by $e^{-\zeta U_0/3}$ while the forward rates are increased by $e^{(1-\zeta)U_0/3}$. In our model, only the backward diffusion rate in the ATP-bound state can be reduced somewhat by this potential (see details in SI).

Results on translocation

Translocation velocity

Using the two-state representation and translocation scheme in Fig. 2a, one can derive via a chemical master equation the average translocation velocity in the steady state (see SI). By assuming that (i) the forward transition a→b is rate limited by ATP binding ($\omega_{ab}^{I}=k_{ET}\cdot[ATP]$) while the forward transition b→a is rate limited by domain 2 movement that couples with hydrolysis product release ($\omega_{ba}^{II}=k_{cat}$), (ii) the reverse backward transitions are slow enough ($\omega_{ba}^{I}\ll\omega_{ab}^{I}$, $\omega_{ab}^{II}\ll\omega_{ba}^{II}$), and (iii) the diffusion rate in the apo state is negligible ($r_a\to 0$), while the diffusion rate in the ATP-bound state is significant ($r_b>0$), we obtain the following expression for the average translocation velocity:

$$v^{\text{trans}}=l_0\frac{k_{\text{cat}}\cdot[\text{ATP}]}{\frac{k_{\text{cat}}}{k_{\text{ET}}}+[\text{ATP}]} \tag{3}$$

Here $l_0=1$ bp is the periodicity of the helicase movement. Equation (3) has a form of a Michaelis–Menten-like dependence on ATP concentration and is independent of the diffusion rate. We used $k_{\text{cat}}\sim 200\ \text{s}^{-1}$ for ssRNA translocation estimated from single-molecule experiments[41] and an ATP binding rate constant $k_{\text{ET}}\sim 1\ \mu\text{M}^{-1}\ \text{s}^{-1}$ (see SI on parameter tuning and Table S1). In Fig. 3a, we plot the average translocation velocity *versus* [ATP], with $v_{\max}^{\text{trans}}=l_0k_{\text{cat}}\sim 200$ bp/s and $K_m=\frac{k_{cat}}{k_{ET}}\sim 200\mu M$. We will see later that the Michaelis–Menten form of the velocity is maintained during NS3 unwinding, while both $v_{\max}^{\text{trans}}$ and K_{m} become smaller and sequence dependent. Notice also that the rate $k_{\text{cat}}\sim 200\ \text{s}^{-1}$ used above can be regarded as an upper bound for the NS3 translocation.[41] It is much larger than that measured recently from bulk experiments,[20–22] in which different protein states are likely mixed.

We can define a measure of the 'stepping efficiency', e_f, as the number of nucleotides translocated by the helicase in one ATP cycle.[48] Based on structural studies, we have assumed that the helicase domain steps 1 nt at a time.[29] With the use of the average velocity expression Eq. (3), the average stepping efficiency of the helicase translocation, according to Eq. (4), is always 1 nt/ATP:

$$\bar{e}_{\text{f}}\equiv\frac{v^{\text{trans}}\cdot t}{n_{\text{ATP}}}=v^{\text{trans}}\cdot\tau=v^{\text{trans}}\cdot\left(\frac{1}{k_{\text{ET}}\cdot[\text{ATP}]}+\frac{1}{k_{\text{cat}}}\right) \tag{4}$$

where n_{ATP} is the number of ATPs consumed in time t and τ is the average time for one ATP cycle. Note that $\bar{e}_f$ is indeed the inverse of the ATP-coupling stoichiometry (ATP/nt) commonly measured. As a

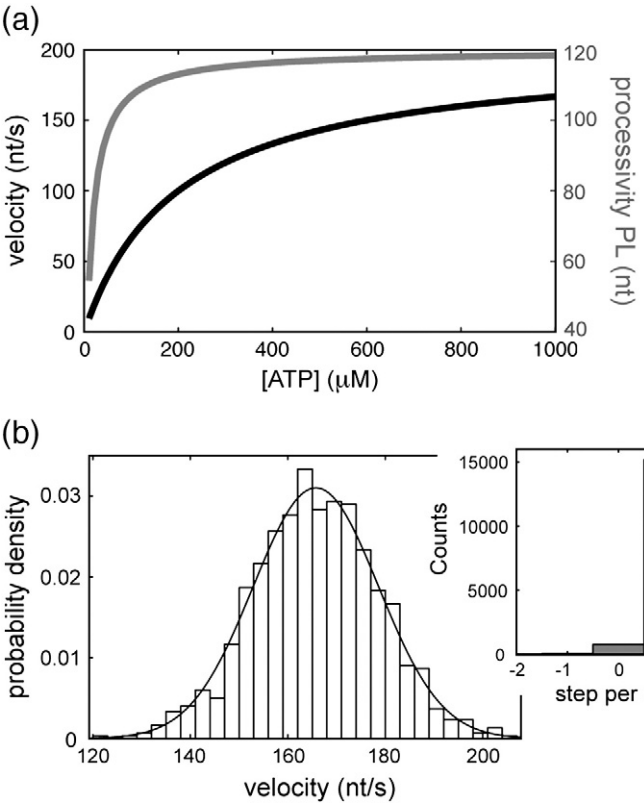

Fig. 3. Translocation properties of NS3 computed from the model. (a) The average translocational velocity and processivity length *versus* [ATP]. For the velocity, v_{max} is 200 bp/s (an upper bound value) and K_m is about 200 μM (when $k_{ET} \sim 1\ \mu M^{-1}\ s^{-1}$) in this case. The processivity length (PL) is close to its maximum (~120 bp) over a large range of [ATP]. (b) Distributions of ss translocation velocity and stepping efficiency. The velocity distribution is taken over an ensemble of trajectories for 1 s each at [ATP]=1 mM, generated from numerical simulation. The average velocity is ~165 nt/s, while the standard deviation is ~12 nt/s. The width of the distribution, that is, the standard deviation, can also be derived from the effective diffusion constant (see the text). The measure of stepping efficiency, defined as steps (nucleotides) translocated per ATP cycle, averages at 1 nt/ATP during the ss translocation. A larger diffusion rate r_b would broaden the distributions (shown in Fig. S3b).

matter of fact, if a higher-order 'sequence effect' of the ss translocation is considered[22] (as mentioned in the Introduction), the average stepping efficiency can drop slightly lower than 1 nt/ATP. Later on, we will show that during duplex unwinding, the average efficiency $\bar{e}_f$ drops well below 1 bp/ATP due to a 'wall' effect: the duplex end base pair, when closed, transiently blocks the helicase translocation and leads to futile ATP cycles. A similar effect applies also to sequence-dependent translocation: when the next sequence barrier is higher than the current one, $\bar{e}_f$ drops below 1 nt/ATP due to futile ATP cycles; otherwise, $\bar{e}_f$ remains at 1 nt/ATP. Overall, the stepping efficiency would be slightly lower than 1 nt/ATP if higher-order sequence effects are detectable during helicase translocation. This measure of the stepping efficiency can be tested experimentally.

Currently, direct measurements of NS3 translocation at the single-molecule level have not been systematically conducted. The results provided here—such as the average velocity and efficiency presented above, as well as the effective diffusion and processivity properties discussed below—are testable, qualitatively and semiquantitatively, in future experiments. A similar form of translocation velocity had been derived in Ref. 40 based on the 'Brownian motor' (or 'flashing ratchet') scheme,[34] in which the helicase does not step when a→b, but jumps 1 nt forward when b→a. In our current scheme, however, the helicase as a whole effectively moves 1/2 nt at a time because domains 1 and 2 move forward 1 nt, respectively, for a→b and b→a. The two schemes give similar kinetic results, but the current scheme has a clearer structural and mechanistic basis.[29,30]

Translocational fluctuations

In SI, we derive effective diffusion constant D_{eff}[49,50] for NS3 ss translocation:

$$D_{eff} \equiv \frac{\langle x^2\rangle - \langle x\rangle^2}{2t} = \frac{k_{cat}\left\{\left(\frac{k_{cat}}{k_{ET}}\right)^2 + [ATP]^2\right\}[ATP]}{2\left(\frac{k_{cat}}{k_{ET}} + [ATP]\right)^3} + \frac{r_b[ATP]}{\frac{k_{cat}}{k_{ET}} + [ATP]} \quad (5)$$

where the average is taken over an ensemble of trajectories. D_{eff} characterizes the randomness arising from both chemical kinetics (the first term in the above equation) and spatial diffusion (the second term) and is proportional to velocity fluctuations measured over a certain time interval ($\sigma_v^2 \equiv \frac{var(x)}{t^2} = \frac{2D_{eff}}{t}$, where σ_v is the standard deviation of the velocities). The results show that D_{eff} increases as [ATP] or any of the parameters, k_{ET}, k_{cat}, or r_b, increases (see Fig. S3a). Hence, the width of the

velocity distribution also increases with [ATP], k_{ET}, k_{cat}, and r_b. Notice that the spatial diffusion (r_b) of the helicase is not evident in the average velocity [Eq. (3)] but can be revealed from measuring D_{eff} or the velocity fluctuations (see Fig. 3b). In our model, we used $r_b = 10\ s^{-1}$, which was estimated to an order of magnitude by examining the velocity fluctuations during unwinding in comparison with experimental data[18,41] (see next section and SI). A more straightforward way of measuring r_b experimentally is to measure D_{eff} or the velocity fluctuations during helicase translocation.

Additionally, we conducted kinetic Monte Carlo simulations[51,52] under the above translocation scheme and calibrated the simulations with analytic derivations [see SI and Eqs. (S1) to (S3)]. With $r_b = 10\ s^{-1}$, the distributions of the translocation velocity (measured for 1000 trajectories of 1 s each at [ATP] = 1 mM) and the stepping efficiency (nucleotides per ATP cycle) are shown in Fig. 3b. A larger r_b ($100\ s^{-1}$) leading to broader distributions of these quantities are shown in Fig. S3b.

Translocation processivity

We also examined processivity of NS3 during translocation by taking into account dissociation events of the helicase as it translocates. We define k_{off}^a and k_{off}^b as two dissociation (off) rates of the NS3 during translocation, in the apo and ATP-bound state, respectively. Since the affinity of the NS3 to the ss is much weaker in the ATP-bound state than in the apo state, we set $k_{off}^a < k_{off}^b$. In this way, the processivity length (PL), that is, the average distance the helicase has traveled along the ss before dissociation, can be written as (see SI):

$$PL^{trans} \equiv \frac{v^{trans}}{k_{off}} = \frac{\frac{k_{cat}}{k_{off}^b} \cdot [ATP]}{\frac{k_{cat}}{k_{ET}} \cdot \frac{k_{off}^a}{k_{off}^b} + [ATP]} \quad (6)$$

where k_{off} is an average (between states a and b) dissociation rate during translocation. PL^{trans} *versus* [ATP] also has a 'Michaelis–Menten' form, with a maximum value k_{off}^b. The dissociation rate k_{off}^b is estimated $\sim 1.7\ s^{-1}$ using $PL^{trans} \leq 120$ bp (unpublished data). The value of k_{off}^a is unknown but can be obtained by measuring PL^{trans} at a low ATP concentration. Using $k_{off}^a = 0.1\ s^{-1}$ in Fig. 3a, it shows that PL^{trans} reaches its half-maximum at a relatively low K_m^{PL} ($\sim 12\ \mu M$), while above [ATP] $\sim 200\ \mu M$, PL^{trans} varies little with [ATP].

Results on unwinding

Michaelis–Menten form of the unwinding velocity

We simulated the unwinding kinetics of the helicase when it translocates or binds to the duplex region (Fig. 2b and Fig. S2), taking into account the base-pair-unwinding potential and junction-stabilizing potential to modulate the forward and backward rates. Under our simulation scheme, we derived approximate solutions that describe well the simulated unwinding behaviors (see details in SI). Our results show that the average unwinding velocity can be approximated as:

$$v^{uwd} = \varepsilon_f l_0 \frac{k_{cat} e^{-\kappa \cdot \Delta G_0} [ATP]}{\frac{k_{cat} e^{-\kappa \cdot \Delta G_0}}{k_{ET}} + [ATP]} \quad (7)$$

Here, ε_f is an average efficiency factor ($0 < \varepsilon_f < 1$) that we will discuss below, $l_0 = 1$ bp is the periodicity, and k_{ET} and k_{cat} are the ATP binding and product catalysis/release (in coupling with the front domain movement) rate of the helicase. ΔG_0 is the base pair stabilizing free energy (the free-energy difference between the base pair open and closed states), and $\kappa \equiv \xi(1-\lambda)$, a constant depending on how active the helicase is ($0 \leq \lambda \leq 1$) and how large the base-pair-unwinding potential reduces the forward rate ($0 < \xi < 1$).

Except for a lowered average efficiency ($\varepsilon_f < 1$), the above unwinding velocity has a Michaelis–Menten form similar to that of the translocation, in which only the effective 'catalytic' rate is reduced ($k_{cat} e^{-\kappa \cdot \Delta G_0}$). This is because at the dominant configuration of the NS3 unwinding ($x_2 = x_0 - 1$ and $x_1 = x_0 - 6$ or 7 in the b or a state, respectively; see SI), the rate k_{cat} that determines how fast the front domain moves forward, in coupling with hydrolysis products release, is reduced by the base-pair-unwinding potential (according to $k_+ = k_+^0 e^{-\xi(1-\lambda)\Delta G_0}$). From the above unwinding velocity, one obtains a sequence-dependent Michaelis constant that is smaller than that being measured in ss translocation: $K_m^{uwd} = \frac{k_{cat}}{k_{ET}} e^{-\kappa \Delta G_0}$; the more stable the sequence (i.e., the larger the ΔG_0), the smaller the K_m^{uwd}. In order to fit with experimental data, we set $\xi = \frac{1}{3} log\left(\frac{k_{cat}}{100 k_{ET}}\right) / (1-\lambda)$ for the NS3 helicase as $\lambda \neq 1$, that is, $\kappa \equiv \xi(1-\lambda) = \frac{1}{3} log\left(\frac{k_{cat}}{100 k_{ET}}\right)$. In this way, we can get $K_m^{uwd} \sim 100\ \mu M$ for $\Delta G_0 \sim 3\ k_B T$, as experimentally measured for NS3 unwinding on a mixed (52% GC) RNA sequence.[18]

Notice that in a situation when ATP binding generates the unwinding force rather than the ATP hydrolysis/product release step, k_{ET} can be reduced to $k_{ET} e^{-\kappa \cdot \Delta G_0}$ upon the base-pair-unwinding potential while k_{cat} remains constant. In that situation, $K_m^{uwd} = \frac{k_{cat}}{k_{ET}} e^{\kappa \Delta G_0}$ should be larger than that being measured under ss translocation [$K_m = \frac{k_{cat}}{k_{ET}} \sim 200 \mu M$ from Eq. (3)]. Moreover, the more stable the sequence to be unwound (the larger the ΔG_0), the larger the K_m^{uwd}. Hence, by comparing experimentally the Michaelis constant measured during unwinding with that in ss translocation, and by examining the sequence dependence of the K_m^{uwd}, it

would be possible to test from future experiments if the unwinding force is generated after hydrolysis product release or during ATP binding.

In Fig. 4a, we show the unwinding velocities of the NS3 helicase *versus* [ATP] calculated for various sequences using Eq. (7). The RNA sequences 100% AU, 100% GC, and mixed (52% GC) are taken from experiments,[18,41] with $\Delta G_0^{AU} = 1.5 \pm 0.5\ k_BT$, $\Delta G_0^{GC} = 4.0 \pm 1.0\ k_BT$, and $\Delta G_0^{mixed} = 3.0 \pm 1.0\ k_BT$[53] for each sequence on average, at close to experimental ionic conditions (see SI). Note that the ΔG_0 we used counts not only hydrogen-bonding interactions within the base pair but also stacking interactions between neighboring base pairs.[54,55] In our calculations, the

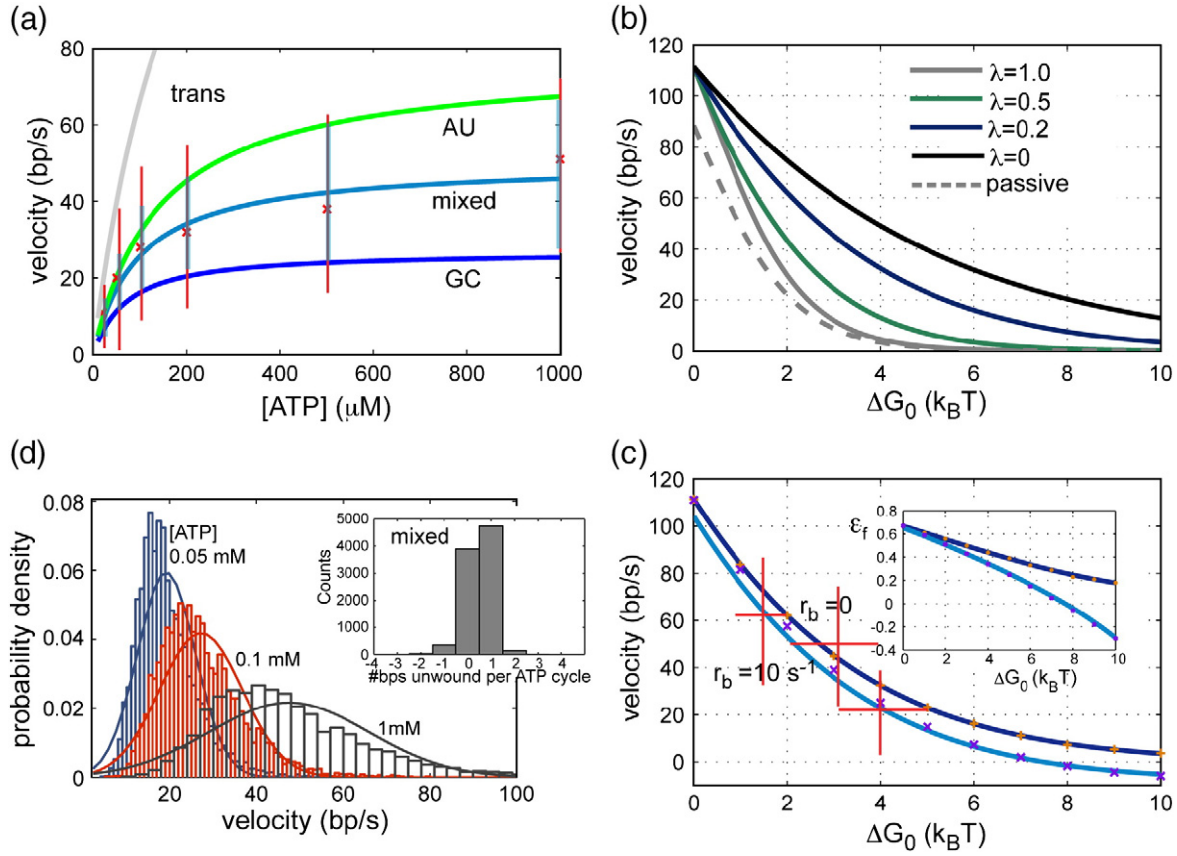

Fig. 4. The unwinding velocity and efficiency of NS3 computed from the model. (a) The velocity *versus* [ATP] of the NS3 as it unwinds different RNA sequences. The 100% GC sequence, the mixed (52% GC), and the 100% AU sequence were adopted from the single-molecule experiments.[18,41] The average values of the velocities were calculated from Eq. (7). The experimentally measured velocities of unwinding the mixed sequence along with the measured error bars (standard deviations) are shown in red. The corresponding error bars calculated from our simulations are shown in light blue. Note that velocity distributions, simulated on unwinding the mixed sequence, are shown in (d). The unwinding velocities are all significantly lower than the translocation velocities and show a Michaelis–Menten dependence on [ATP], with sequence-dependent v_{max} and K_m. (b) The sequence dependence of the unwinding velocity at various helicase 'activeness' (with $r_b = 0$ and [ATP] = 1 mM). The sequence stability is measured by ΔG_0, the base pair stabilizing free energy. The activeness of the helicase unwinding is characterized by $\lambda (0 \le \lambda \le 1)$; the smaller the λ, the more active the helicase and the larger the unwinding velocities. A passive unwinding is a special situation of $\lambda = 1$ (see the text). (c) The sequence dependence of unwinding velocity in the absence and presence of translocation diffusion ($r_b = 0$ and $r_b = 10\ s^{-1}$, both with $\lambda = 0.2$ at [ATP] = 1 mM). The data points were taken from numerical simulations while the curves are drawn from the approximate solution [Eq. (S10) in SI]. Experimental data for the AU ($\Delta G_0 \sim 1.5\ k_BT$), the mixed ($\Delta G_0 \sim 3\ k_BT$), and the GC ($\Delta G_0 \sim 4\ k_BT$) sequences are shown in red.[41] The inset shows the sequence dependence of the average unwinding efficiency (ε_f) with $r_b = 0$ (dark blue) and $r_b = 10\ s^{-1}$ (light blue). (d) The distributions of the unwinding velocity and unwinding efficiency (of the mixed sequence) from numerical simulations. The velocity distributions were taken at [ATP] = 0.05, 0.1, and 1 mM in order to compare with experimental data.[18] The average and standard deviation of the distribution, from both the simulation and experimental data, are shown in (a). The distributions show some deviations from the Gaussian fit (curves). The standard deviation of each distribution has been shown in (a) at corresponding [ATP] (light blue error bar). The unwinding efficiency is defined as the number of base pairs unwound per ATP cycle. The histogram is collected from a long trajectory ($t = 100$ s) with $\lambda = 0.2$, $r_b = 10\ s^{-1}$ at [ATP] = 1 mM. The same values of λ and r_b are utilized also in (a); unless specified, these values are used by default through this work.

velocities are the same whether we used the above average ΔG_0 for the sequence according to Eq. (7) or we adopted variable ΔG_0 for each base pair along the sequence and simulated the unwinding numerically. The results in Fig. 4a show that the larger the sequence barrier (ΔG_0), the lower the velocity curve and the lower the K_m^{uwd}, which is ~140 μM, 100 μM, and 40 μM for the sequence AU, mixed, and GC, respectively. In particular, the experimental data (red)[18] for unwinding the mixed sequence are shown, with our fitted results. The main parameter values we used in the calculations are specified later (see all parameter values in Table S1 in SI).

Sequence dependence and active unwinding

In Eq. (7), the sequence dependence of the unwinding velocity resides not only in the reduced forward rate k_{cat} but also in the average efficiency factor ε_f, which can be regarded as the probability that the base pair opens when the helicase front domain reaches to the duplex end ($x_2 = x_0$). In a simple case when $r_b = 0$, this efficiency factor can be written as:

$$\varepsilon_f = P_{open} + \left(1 - P_{open}\right) \cdot P_{switch} \tag{8}$$

where $P_{open} = \frac{e^{-\lambda \cdot \Delta G_0}}{1 + e^{-\lambda \cdot \Delta G_0}}$ accounts for the base pair opening probability under the helicase action, with the base pair stabilizing free energy reduced to $\lambda \Delta G_0$. $P_{switch} = \frac{e^{-\lambda \Delta G_0 - \delta_A}}{1 + e^{-\lambda \Delta G_0 - \delta_A}}$ accounts for an additional probability of opening the base pair, by switching the base pair from the closed state to the open state as the helicase uses an extra energy to immediately cross the activation barrier $\lambda \Delta G_0 + \delta_A$ (see Fig. 2b). Note that when δ_A is large, P_{switch} is close to zero. Hence, when $\delta_A \to \infty$ and $\lambda = 1$, the unwinding becomes passive; that is, the helicase proceeds only when the base pair spontaneously opens,[46] leading to $v_{passive}^{uwd} = \frac{e^{-\Delta G_0}}{1 + e^{-\Delta G_0}} v^{trans}$.

The sequence dependence of the unwinding velocity (with $r_b = 0$ and $\delta_A = 1\ k_BT$ at [ATP] = 1 mM) is shown in Fig. 4b. One can see that the smaller the λ, that is, the more active the helicase, the larger the unwinding velocity, and the slower the velocity approaches to zero as ΔG_0 increases (i.e., smaller sequence dependence). On the other hand, for a helicase not active enough ($\lambda \to 1$), its velocity can approach zero when ΔG_0 is fairly small. In that case, the helicase would stall at the DNA/RNA junction without being able to proceed further. This may explain why some helicases, like monomeric Rep,[32] cannot unwind duplex DNA though it can translocate well along ssDNA. Notice that when $\Delta G_0 \to 0$ (base pair opening and closing are equally alike), with the activation barrier $\delta_A = 1\ k_BT$ relatively small, the unwinding velocities for all active cases converge to ~111 bp/s (with $k_{cat} = 200\ s^{-1}$ and other default parameter values in this model, see Table S1); while for the passive case, the average velocity is about 88 bp/s at $\Delta G_0 \to 0$, which is half of the translocation velocity at this ATP concentration, detectably lower than any active case.

When $r_b \neq 0$, the diffusional flux decreases ε_f. Since the forward diffusion rate r_b^+ is reduced significantly upon unwinding, while the backward diffusion r_b^- is affected less, a negative velocity flux results [see the approximate solution Eq. (S10) in SI]. Hence, ε_f depends not only on the sequence stability (ΔG_0) and how active the helicase is (λ) but also on the diffusional property of the helicase along the nucleic acid track (r_b). Figure 4c shows the unwinding velocity and the efficiency factor *versus* ΔG_0 for both $r_b = 0$ and $r_b = 10\ s^{-1}$, with $\delta_A = 1\ k_BT$ and $\lambda = 0.2$ at [ATP] = 1 mM. One can see that the larger the ΔG_0, r_b, or λ, the smaller the velocity and the efficiency. When r_b is relatively large ($r_b = 10\ s^{-1}$), the sequence dependence of the unwinding efficiency (in base pair per ATP for ε_f times l_0) is more significant than when $r_b = 0$ (inset in Fig. 4c). The sequence dependence of the unwinding efficiency can be tested experimentally.

Unwinding characteristics and fluctuation properties

In Fig. 4c, we also show the experimental data (red)[41] on NS3 unwinding of AU, mixed, and GC sequence at [ATP] = 1 mM, which can be fitted well with parameters $\delta_A = 1\ k_BT$, $\lambda = 0.2$, and $r_b = 10\ s^{-1}$ (see Table S1). The activation barrier δ_A for the RNA end base pair open⇒close transition is not known exactly, but its upper bound value is about 10 k_BT.[56] We tested a range of δ_A (from 0 to 10 k_BT) and found that λ can always be tuned to 0.1–0.3 by fitting the unwinding velocity at a specific value of ΔG_0. Further, by varying ATP binding rate constant k_{ET} within its range ($0.1 < k_{ET} < 2\ \mu M^{-1}\ s^{-1}$, see SI and Table S1), λ varies between 0 and 0.5. In principle, λ does not have to be the same for different sequences, but our results show that tuning λ for the AU, mixed, and GC individually led to similar or identical λ. In addition, by considering the noise/fluctuations (second moment) of the unwinding velocities besides the average values measured from the single-molecule experiments,[18,41] we found that $r_b = 10\ s^{-1}$ recovers about 50% to 90% of the measured noise, while the upper bound of r_b is lower than 50 s^{-1}. Details on choosing appropriate parameters for the current model are provided in SI, Table S1, Table S2, and related text. These results indicate that NS3 is a very active helicase ($\lambda < 0.5$); on the other hand, the diffusion/fluctuation character of NS3 is significant ($r_b \sim 10\ s^{-1}$) and adversely affects its unwinding efficiency.

In Fig. 4d, we show distributions of unwinding velocities of the NS3 helicase on the mixed RNA sequence, obtained from simulating an ensemble

($N=1000$) of trajectories at [ATP]=1 mM (gray), 0.1 mM (red), and 0.05 mM (blue). These distributions are similar to the experimental measurements obtained in Fig. 2c of Ref. 18. The standard deviations of the velocity distributions calculated at different [ATP] are shown in Fig. 4a (light blue error bars), which are about 50–90% the experimental values (red error bars), leaving part of experimentally measured fluctuations to other sources of noise. To be consistent with experimental measurements,[18] we sampled the velocities and fluctuations at every 11 bp (pauses were detected in experiments[18] for about every 11 bp) on the simulated trajectories. Thus, for each sampling, a relatively small number of ATP cycles were included. This short-time velocity sampling, together with the diffusive character of the NS3 helicase ($r_b \sim 10\ s^{-1}$), led to relative broad distributions of velocities. Similar to the translocation case in Fig. 3b, the width of the distribution increases with [ATP] because a higher concentration of ATP leads to a higher probability of the helicase being in the ATP-bound state. This introduces a larger stochasticity (i.e., more diffusive) into the model [see also Eq. (5)]. The distributions also show detectable deviations from a Gaussian distribution (the fitting curve in Fig. 4d), which would otherwise be a good approximation if a large number of ATP cycles (long time) were sampled.

In the inset of Fig. 4d, we also show the distribution of the 'unwinding efficiency', that is, the number of base pairs unwound per ATP cycle for a long trajectory unwinding a mixed RNA sequence ($t=100$ s without considering pauses or helicase dissociation). This is comparable to the 'translocation efficiency', that is, the translocation steps per ATP cycle shown in Fig. 3b. Notice that the efficiency is independent of [ATP] [cf. Eqs. (3), (4) and (7)]. Importantly, compared with translocation, helicase unwinding has a significant number of zero (futile cycles) or even negative steps (under small but nonzero backward rates ω_{ba}^{I} and ω_{ab}^{II}, and under backward diffusion when $r_b>0$) accumulated as net movements for an ATP cycle, leading to an average stepping (unwinding) efficiency e_f lower than 1 bp/ATP (the average efficiency is proportional to the efficiency factor e_f: $e_f \equiv \varepsilon_f \cdot l_0$). That is to say, the average stepping efficiency changes from 1 nt/ATP in the ss translocation to a sequence-dependent value smaller than 1 bp/ATP during unwinding (see ε_f in Fig. 4c). As mentioned before, this is mainly due to the presence of the duplex that interrupts the translocation and leads to occasional futile ATP cycles. The average efficiency also decreases during unwinding when the spatial diffusion increases ($r_b>0$). During ss translocation, the diffusion does not affect the average efficiency but only expands the distribution of the efficiency measure, that is, steps per cycle (see Fig. 3b and Fig. S3b).

Sequence-dependent dissociation

NS3 is not a highly processive helicase[2] due to frequent dissociations from the nucleic acid track. Modeling studies had suggested that active unwinding of the helicase leads to sequence-dependent dissociation.[39] Single-molecule measurements have also identified this behavior.[41] Below, we examine more closely the NS3 dissociation in the two-state model and in the presence of helicase diffusion.

As discussed above, the dissociation rates of the helicase in the ATP-bound and the apo states during translocation are k_{off}^{b} ($\sim 1.7\ s^{-1}$) and k_{off}^{a} ($\ll k_{off}^{b}$), respectively. At the DNA/RNA junction, NS3 is stabilized and the dissociation rate decreases correspondingly to $k_{aff}^{a,b} e^{-U_{a,b}^{0}}$ due to the attractive potential $U_{a,b}^{0}$. During unwinding, the dissociation rate in the individual state would be further modulated to $k_{off}^{a,b} e^{-U_{a,b}^{0}+(1-\lambda)\Delta G_0}$, as the helicase front domain reaches the duplex end ($x_2=x_0$) where the base-pair-unwinding potential $(1-\lambda)\Delta G_0$ peaks (see Fig. 2b).

In Fig. 5a, we show simulation data on the average dissociation rate k_{off}^{uwd} of the NS3 helicase as it unwinds the AU, the mixed, and the GC sequence at various [ATP]. From the diagram, one can see that a higher sequence stability leads to a larger k_{off}^{uwd}, due to the higher sequence barrier $(1-\lambda)\Delta G_0$. For the GC sequence at the high [ATP] (1 mM), we fit the experimental data $k_{off}^{uwd} = 0.5\ s^{-1}$. For the AU sequence at the same condition, we obtained k_{off}^{uwd} about half of that for GC, which agrees very well with experimental results.[41] For each sequence, the lower the [ATP], the lower the k_{off}^{uwd}. This effect occurs because at low [ATP], the helicase spends most its time in the apo state, in which the helicase has a high affinity to the substrate than in the ATP-bound state (see below), and dissociates slower from the nucleic acid than in the ATP-bound state.

Note that the junction stabilization strength in the apo state $U_0^a \sim 4.4\ k_BT$ was estimated from biochemical data[34] (see SI). By fitting $k_{off}^{uwd} = 0.5\ s^{-1}$ on the GC sequence from single-molecule measurements,[41] we obtained $U_0^b \sim 1.8\ k_BT$ in the ATP-bound state (U_0^b ranges 1.3–2 k_BT when parameter k_{ET} varies). Hence, both the larger junction stabilization ($U_0^a > U_0^b$) and the higher ss affinity (smaller ss dissociation rate $k_{off}^{a} < k_{off}^{b}$) in the apo state contribute to the lower dissociation rate in this state and, consequently, to the lower average k_{off}^{uwd} at low [ATP].

The curves of dissociation rate in Fig. 5a also demonstrate Michaelis–Menten-like forms, with the 'Michaelis constant' fit to 78 μM, 70 μM, and 58 μM for the AU, mixed, and GC case, respectively. That is, the Michaelis constant for the dissociation rate also decreases with increasing sequence stability, similarly as that for the unwinding velocity. Therefore, if one calculates the processivity length $PL \equiv \frac{v}{k_{off}}$, one obtains PL relatively insensitive to [ATP] over a large range (see Fig. S4b). Further, from force effects

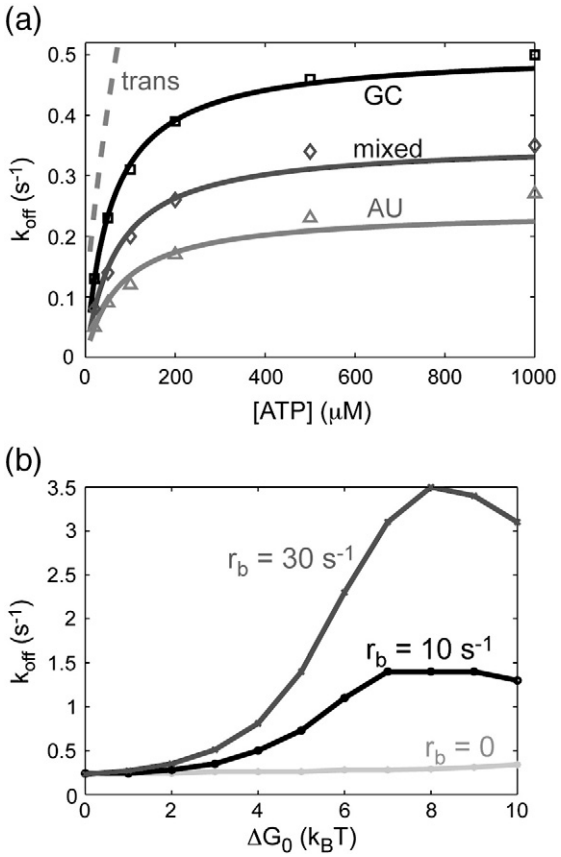

Fig. 5. The dissociation rate of NS3 during active unwinding computed from the model. (a) The dissociation rate *versus* [ATP] for different sequences. The data points were taken from numerical simulations of an ensemble of trajectories ($N=1000$), and the curves are fit to the data points. The dissociation rates show a Michaelis–Menten-like dependence on [ATP] with sequence-dependent characteristics. (b) The sequence dependence of the dissociation rate at different diffusion rates: $r_b=0$, $r_b=10\ s^{-1}$, and $r_b=30\ s^{-1}$. In the absence of the translocation diffusion ($r_b=0$), the sequence dependence is hardly discernable. In the presence of the diffusion ($r_b=10\ s^{-1}$ and $r_b=30\ s^{-1}$), the dissociation rate increases with the sequence stability (ΔG_0) over a large range; the larger the diffusion rate, the larger the sequence dependence.

on the velocity and the dissociation rate (see Fig. S4a), the processivity is expected to rise significantly with the unwinding force; this is consistent with experimental results.[18,57] Nevertheless, NS3 spends a significant amount of time pausing during unwinding,[18] which has not been taken into account here. Thus, the experimentally measured processivity length should be much smaller than the value calculated above.

In Fig. 5b, we plot the sequence dependence of k_{off}^{uwd} at three different values of r_b. At $r_b=10\ s^{-1}$, we see that k_{off}^{uwd} consistently rises as ΔG_0 increases over a large range of values. However, over $\Delta G_0=7$–$10\ k_BT$, k_{off}^{uwd} changes little and then drops; it drops a bit further at $\Delta G_0=10$–$13\ k_BT$ and increases again (data not shown). The non-monotonic behavior of k_{off}^{uwd} *versus* ΔG_0 is due to competition between two effects: (i) the sequence barrier ΔG_0 increases the dissociation rate by $e^{(1-\lambda)\Delta G_0}$, which happens occasionally at $x_2=x_0$; (ii) ΔG_0 also decreases the forward rate (k_{cat} or r_b) of the helicase by $e^{-\kappa\Delta G_0}$ at $x_2=x_0-1$, reducing the chances that the helicase reaches the sequence barrier at $x_2=x_0$. Combining these two effects, ΔG_0 increases the dissociation rate to some extent and then inhibits the rate from growing further. This property can be tested experimentally using sufficiently stable sequences.

In addition, the sequence dependence of the dissociation rate is also affected by the diffusive character of the helicase. When $r_b=0$, there is only a slight increase in k_{off}^{uwd} within $\Delta G_0=0$–$10\ k_BT$ (k_{off}^{uwd} can become bigger for very large ΔG_0, data not shown); when $r_b=30\ s^{-1}$, the change of k_{off}^{uwd} over the same range of ΔG_0 is much bigger than that for smaller r_b. The reason is that, in the absence of the diffusion, the only events through which the helicase reaches the sequence barrier are forward movements of domain 2 upon the hydrolysis products release (in k_{cat}); the presence of the diffusion (in r_b) brings more opportunities for the helicase to reach the sequence barrier. Thus, the larger the r_b, the larger the sequence effect on k_{off}^{uwd}.

Overall, the average dissociation rate of the helicase is affected by several factors during the active unwinding: the probability the helicase being bound with ATP, the sequence stability, and the helicase diffusion rate. The different affinities of the helicase for the ss and ds forms of the nucleic acid, with and without ATP, make the dissociation rate differ between the two states. The dominant sequence effect comes from the base-pair-unwinding potential, that is, the sequence barrier, which may also destabilize the helicase at the junction, fostering dissociation. On the other hand, the sequence barrier resists the helicase approaching the duplex end, additionally affecting the dissociation. Lastly, the diffusive character of the helicase can enhance the sequence effect on helicase dissociation by increasing the frequency of the helicase approaching to the sequence barrier.

Discussion

We have modeled the NS3 helicase activity based on structural[14,29] and biochemical properties.[33,34] A single catalytic site binds ATP between the two translocation domains of the helicase and modulates both interdomain associations and individual domain affinities to the nucleic acid substrate. In particular, the overall affinity of the NS3 to the ss

nucleic acid is significantly reduced in the ATP-bound sate,[33,34] allowing the helicase to diffuse along the ss. When the helicase reaches the RNA/DNA duplex, the forward movement of the helicase front domain induces base pair unwinding. By fitting data on RNA unwinding velocities measured from single-molecule experiments,[18,41] our studies suggest that the NS3 helicase actively shifts the base pair open↔close equilibrium away from the closed state toward the open state. It does this by reducing the free energy stabilizing the base pairing/stacking at the end of the duplex to less than half of its original value.

During active unwinding, the NS3 helicase interacts with the RNA/DNA duplex, perturbing the structure of the duplex as well. The interactions lead to two detectable effects. First, a base-pair-unwinding potential at the duplex end reduces the stepping velocity of the helicase by inhibiting forward movement of the front domain and reducing the average stepping efficiency in comparison with ss translocation. Both of these reductions depend on the DNA/RNA sequence encountered by the front domain. Second, the helicase preferentially associates with the duplex and, thus, is stabilized at the junction. The preferential association may come from interactions of the duplex backbone with the helicase as suggested for PcrA[25,30] and may also be contributed by partial base unstacking at the junction.[47] The junction stabilization reduces the dissociation rate of the helicase during unwinding but does not affect the translocation velocity much. Nevertheless, both the base pair-unwinding and the junction-stabilization effects arise from the helicase interacting with the duplex. It is likely, therefore, that the strengths of the two effects are correlated; that is, the larger the junction stabilization during the ATP hydrolysis cycle, the more active the helicase will be in base pair unwinding. More detailed studies are needed to clarify this issue.

When external forces that assist unwinding are applied to the DNA/RNA duplex, the base pair stabilizing free energy should drop. The model shows how the applied force affects the unwinding velocity and dissociation rate (see Fig. S4). However, the force effects were not detected for NS3 unwinding of RNA in single-molecule experiments.[18,41] This force insensitivity could have been explained during translocation, as some chemical step other than duplex unwinding is rate limiting in the overall mechanochemical cycle of the enzyme. This interpretation is, however, inconsistent with the slowing down of the enzyme observed experimentally when it encounters a sequence rich in GC content.[41] One possible explanation is that the enzyme possesses additional nucleic acid binding sites such that the force does not act directly on the junction or fork of the duplex, but at a different RNA–protein contact. This would prevent the externally applied force from weakening the base pair at the duplex junction.

An important characteristic of the NS3 helicase in this model is that translocational diffusion is not negligible when the helicase is bound with ATP. During ss translocation, the diffusion affects the fluctuation properties of the helicase without impacting the average translocation velocity or the tight coupling between hydrolysis and stepping that produces an average stepping efficiency of 1 nt/ATP. During unwinding, however, the diffusive character does affect both the fluctuation properties and the average velocity/efficiency of the helicase. Even in the absence of diffusion, the unwinding efficiency is lower than 1 bp/ATP due to occasional futile ATP cycles upon the sequence barrier. The diffusion further lowers the average efficiency. The larger the diffusion rate, the more the sequence barrier decreases the efficiency, and this is achieved by increasing the frequency of backward jumps (−1 nt at a time) during unwinding. In the model, significant backward jumps are present when the diffusion rate is non-zero. Our numerical results suggest that the ratio between backward and forward jumps during unwinding increases with sequence stability, for example, from ~10% in unwinding AU to ~30% in unwinding GC (at 1 mM [ATP] with default parameters in Table S1). In future single-molecule experiments, the backward jumps can be better characterized. Hence, the experiments are expected to substantiate and quantify the diffusive character of the helicase.

The interplay between the diffusion and sequence effects is also displayed in helicase dissociation during active unwinding. The helicase's dissociation rate usually increases with increasing sequence stability/barrier. However, a very large sequence barrier may prevent the helicase from reaching the barrier so that the dissociation rate cannot grow monotonically with the strength of the barrier. According to our numerical results, the sequence dependence of the dissociation rate is detectable only in the presence of diffusion; the larger the diffusion rate, the more pronounced the sequence dependence.

To quantify the diffusive character of the NS3 helicase, we estimated the diffusion rate to an order of 10 s^{-1} based on unwinding velocity fluctuations (standard deviation) measured from single-molecule experiments.[18,41] The diffusion rate can also be estimated by measuring the average unwinding efficiency (or the ATP stoichiometry), that is, how many base pairs unwound for each ATP consumed, or vice versa. More straightforwardly, one could obtain the diffusion rate from measuring velocity fluctuation, or effective diffusion rate, during ss translocation of the helicase in single-molecule experiments.

Coupling ss nucleic acid translocation with duplex unwinding is a generic feature of most helicases. In our current unwinding model, the monomeric NS3 helicase shares some common mechanochemical features with the hexameric ring-shaped T7 helicase.[36] For example, the force generation during unwinding for both helicases is likely associated with hydrolysis product (P_i) release, not ATP/dTTP binding.[36,37] Hence, even though their structures are very different, the sequence-dependent effect during unwinding could be similar for these two helicases, as shown in previous experiments.[35] It would be interesting to establish whether the diffusive character of the NS3 helicase is shared by other nucleic acids motors and to investigate how diffusion may impact their function.

According to most recent structural studies,[29] the fundamental or physical step size of the NS3 helicase should be 1 nt at a time. This property should be measurable in future single-molecule experiments with sufficiently high resolution. Note that this 1-nt physical step leads to an average stepping efficiency less than 1 bp per ATP cycle in our model during unwinding and to a broadened distribution involving several base pairs forward or backward per ATP cycle (i.e., the net or total movement of the helicase within one ATP cycle). Nevertheless, our current work cannot explain the 3-bp periodic steps detected in single-molecule fluorescence experiments for NS3 in DNA unwinding[42] or the regular pauses displayed by NS3 about every 11 bp during RNA unwinding in single-molecule optical tweezer experiments.[18]

The 11-bp step may correspond to the binding of the third domain of the protein to the duplex region some 10 or 11 bp away from the fork. As suggested by single-molecule experiments,[18,41] the third domain may be used both as an anchor for the enzyme and as a way of locally destabilizing the duplex ahead of the fork. This would facilitate inchworming of the other two domains of the protein during unwinding. Furthermore, additional binding sites of NS3 to nucleic acids have been suggested,[43,44] and this could explain the force insensitivity of the unwinding rate observed in single-molecule experiments.[18] In particular, positively charged areas seem to extend from the exterior side of domains 3 and 2 to the protease part of NS3,[43,44] providing attractive interactions for the DNA/RNA strand. Hence, the associations between the helicase and the nucleic acid may block an externally applied force from affecting the stability of the duplex at the fork, and it may also explain the pausing and stepping behaviors displayed by the helicase. It is also possible that the helicase employs a 'scrunching' mechanism as has been suggested for UvrD helicase.[58] This could also lead to complex pausing and stepping behaviors. Further studies will be needed to clarity these issues.

Materials and Methods

In the SI, we show in detail (a) how we derive the helicase binding configuration at the junction, (b) how we use master equation approach to obtain translocation properties of the helicase, (c) how we simulate helicase unwinding dynamics and derive approximate solutions, and (d) how we tune parameters in this model.

Acknowledgements

J.Y. was supported by University of California Berkeley Chancellor's postdoctoral fellowship. G.O. was supported by National Science Foundation Grant DMS 0414039.

Supplementary Data

Supplementary data associated with this article can be found, in the online version, at doi:10.1016/j.jmb.2010.09.047

References

1. Singleton, M. R., Dillingham, M. S. & Wigley, D. B. (2007). Structure and mechanism of helicases and nucleic acid translocases. *Annu. Rev. Biochem.* **76**, 23–50.
2. Pyle, A. M. (2008). Translocation and unwinding mechanisms of RNA and DNA helicases. *Annu. Rev. Biophys.* **37**, 317–336.
3. Enemark, E. J. & Joshua-Tor, L. (2008). On helicases and other motor proteins. *Curr. Opin. Struct. Biol.* **18**, 243–257.
4. Tuteja, N. & Tuteja, R. (2004). Unraveling DNA helicases. *Eur. J. Biochem.* **271**, 1849–1863.
5. Jankowsky, E. & Fairman, M. E. (2007). RNA helicases—one fold for many functions. *Curr. Opin. Struct. Biol.* **17**, 316–324.
6. Gorbalenya, A. E. & Koonin, E. V. (1993). Helicases: amino acid sequence comparisons and structure–function relationships. *Curr. Opin. Struct. Biol.* **3**, 419–429.
7. Lohman, T. M., Tomko, E. J. & Wu, C. G. (2008). Non-hexameric DNA helicases and translocases: mechanisms and regulation. *Nat. Rev., Mol. Cell Biol.* **9**, 391–401.
8. Cox, M. M. (2007). Motoring along with the bacterial RecA protein. *Nat. Struct. Mol. Biol.* **8**, 127–138.
9. Thomsen, N. D. & Berger, J. M. (2008). Structural frameworks for considering microbial protein- and nucleic acid-dependent motor ATPases. *Mol. Microbiol.* **69**, 1071–1090.
10. Patel, S. S. & Picha, K. M. (2000). Structure and function of hexameric helicases. *Annu. Rev. Biochem.* **69**, 651–697.
11. Wang, J. (2004). Nucleotide-dependent domain motions within rings of the RecA/AAA+ superfamily. *J. Struct. Biol.* **148**, 259–267.

12. Frick, D. N. (2007). The hepatitis C virus NS3 protein: a model RNA helicase and potential drug target. *Curr. Issues Mol. Biol.* **9**, 1–20.
13. Yao, N., Hesson, T., Cable, M., Hong, Z., Kwong, A. D., Le, H. V. & Weber, P. C. (1997). Structure of the hepatitis C virus RNA helicase domain. *Nat. Struct. Mol. Biol.* **4**, 463–467.
14. Kim, J. L., Morgenstern, K. A., Griffith, J. P., Dwyer, M. D., Thomson, J. A., Murcko, M. A. *et al.* (1998). Hepatitis C virus NS3 RNA helicase domain with a bound oligonucleotide: the crystal structure provides insights into the mode of unwinding. *Structure*, **6**, 89–100.
15. Cho, H. S., Ha, N. C., Kang, L. W., Chung, K. M., Back, S. H., Jang, S. K. & Oh, B. H. (1998). Crystal structure of RNA helicase from genotype 1b hepatitis C virus. *J. Biol. Chem.* **273**, 15045–15052.
16. Raney, K. D., Sharma, S. D., Moustafa, I. M. & Cameron, C. E. (2010). Hepatitis C virus non-structural protein 3 (HCV NS3): a multifunctional antiviral target. *J. Biol. Chem.* **285**, 22725–22731.
17. Levin, M. K., Wang, Y. H. & Patel, S. S. (2004). The functional interaction of the hepatitis C virus helicase molecules is responsible for unwinding processivity. *J. Biol. Chem.* **279**, 26005–26012.
18. Dumont, S., Cheng, W., Serebrov, V., Beran, R. K., Tinoco, I., Pyle, A. M. & Bustamante, C. (2006). RNA translocation and unwinding mechanism of HCV NS3 helicase and its coordination by ATP. *Nature*, **439**, 105–108.
19. Jennings, T. A., Mackintosh, S. G., Harrison, M. K., Sikora, D., Sikora, B., Dave, B. *et al.* (2009). NS3 helicase from the hepatitis C virus can function as a monomer or oligomer depending on enzyme and substrate concentrations. *J. Biol. Chem.* **284**, 4806–4814.
20. Matlock, D. L., Yeruva, L., Byrd, A. K., Mackintosh, S. G., Langston, C., Brown, C. *et al.* (2010). Investigation of translocation, DNA unwinding, and protein displacement by NS3h, the helicase domain from the hepatitis C virus helicase. *Biochemistry*, **49**, 2097–2109.
21. Rajagopal, V., Gurjar, M., Levin, M. K. & Patel, S. S. (2010). The protease domain increases the translocation stepping efficiency of the hepatitis C virus NS3-4A helicase. *J. Biol. Chem.* **285**, 17821–17832.
22. Khaki, A. R., Field, C., Malik, S., Niedziela-Majka, A., Leavitt, S. A., Wang, R. *et al.* (2010). The macroscopic rate of nucleic acid translocation by hepatitis C virus helicase NS3h is dependent on both sugar and base moieties. *J. Mol. Biol.* **400**, 354–378.
23. Mackintosh, S. G. & Raney, K. D. (2006). DNA unwinding and protein displacement by superfamily 1 and superfamily 2 helicases. *Nucleic Acids Res.* **34**, 4154–4159.
24. Eargle, J., Wright, D. & Luthey-Schulten, Z. (2006). Multiple alignment of protein structures and sequences for VMD. *Bioinformatics*, **22**, 504–506.
25. Velankar, S. S., Soultanas, P., Dillingham, M. S., Subramanya, H. S. & Wigley, D. B. (1999). Crystal structures of complexes of PcrA DNA helicase with a DNA substrate indicate an inchworm mechanism. *Cell*, **97**, 75–84.
26. Korolev, S., Lohman, T. M., Waksman, G., Yao, N. & Weber, P. C. (1998). Comparisons between the structures of HCV and Rep helicases reveal structural similarities between SF1 and SF2 super-families of helicases. *Protein Sci.* **7**, 605–610.
27. Humphrey, W., Dalke, A. & Schulten, K. (1996). VMD: visual molecular dynamics. *J. Mol. Graphics*, **14**, 33–38.
28. Russell, R. B. & Barton, G. J. (1992). Multiple protein sequence alignment from tertiary structure comparison: assignment of global and residue confidence levels. *Proteins: Struct. Funct. Genet.* **14**, 309–323.
29. Gu, M. & Rice, C. M. (2010). Three conformational snapshots of the hepatitis C virus NS3 helicase reveal a ratchet translocation mechanism. *Proc. Natl Acad. Sci. USA*, **107**, 521–528.
30. Yu, J., Ha, T. & Schulten, K. (2006). Structure-based model of the stepping motor of PcrA helicase. *Biophys. J.* **91**, 2097–2114.
31. Yu, J., Ha, T. & Schulten, K. (2007). How directional translocation is regulated in a DNA helicase motor. *Biophys. J.* **93**, 3783–3797.
32. Brendza, K. M., Cheng, W., Fischer, C. J., Chesnik, M. A., Niedziela-Majka, A. & Lohman, T. M. (2005). Autoinhibition of *Escherichia coli* Rep monomer helicase activity by its 2B subdomain. *Proc. Natl Acad. Sci. USA*, **102**, 10076–10081.
33. Levin, M. K., Gurjar, M. M. & Patel, S. S. (2003). ATP binding modulates the nucleic acid affinity of hepatitis C virus helicase. *J. Biol. Chem.* **278**, 23311–23316.
34. Levin, M. K., Gurjar, M. M. & Patel, S. S. (2005). A Brownian motor mechanism of translocation and strand separation by hepatitis C virus helicase. *Nat. Struct. Mol. Biol.* **12**, 429–435.
35. Donmez, I., Rajagopal, V., Jeong, Y. J. & Patel, S. S. (2007). Nucleic acid unwinding by hepatitis C virus and bacteriophage T7 helicases is sensitive to base pair stability. *J. Biol. Chem.* **282**, 21116–21123.
36. Donmez, I. & Patel, S. S. (2008). Coupling of DNA unwinding to nucleotide hydrolysis in a ring-shaped helicase. *EMBO J.* **27**, 1718–1726.
37. Wang, Q., Arnold, J. J., Uchida, A., Raney, K. D. & Cameron, C. E. (2010). Phosphate release contributes to the rate-limiting step for unwinding by an RNA helicase. *Nucleic Acids Res.* **38**, 1312–1324.
38. Betterton, M. D. & Julicher, F. (2005). Opening of nucleic-acid double strands by helicases: active versus passive opening. *Phys. Rev. E: Stat. Nonlin. Soft Matter Phys.* **71**, 011904.
39. Betterton, M. D. & Julicher, F. (2005). Velocity and processivity of helicase unwinding of double-stranded nucleic acids. *J. Phys.: Condens. Matter, S3851.*
40. Garai, A., Chowdhury, D. & Betterton, M. D. (2008). Two-state model for helicase translocation and unwinding of nucleic acids. *Phys. Rev. E: Stat. Nonlin. Soft Matter Phys.* **77**, 061910.
41. Cheng, W., Dumont, S., Tinoco, I. & Bustamante, C. (2007). NS3 helicase actively separates RNA strands and senses sequence barriers ahead of the opening fork. *Proc. Natl Acad. Sci. USA*, **104**, 13954–13959.
42. Myong, S., Bruno, M. M., Pyle, A. M. & Ha, T. (2007). Spring-loaded mechanism of DNA unwinding by hepatitis C virus NS3 helicase. *Science*, **317**, 513–516.
43. Serebrov, V., Beran, R. K. F. & Pyle, A. M. (2009). Establishing a mechanistic basis for the large kinetic steps of the NS3 helicase. *J. Biol. Chem.* **284**, 2512–2521.
44. Beran, R. K. F., Serebrov, V. & Pyle, A. M. (2007). The serine protease domain of hepatitis C viral NS3 activates

RNA helicase activity by promoting the binding of RNA substrate. *J. Biol. Chem.* **282**, 34913–34920.
45. Chen, Y. Z., Zhuang, W. & Prohofsky, E. W. (1992). Energy flow considerations and thermal fluctuational opening of DNA base pairs at a replicating fork: unwinding consistent with observed replication rates. *J. Biomol. Struct. Dyn.* **10**, 415–427.
46. Lohman, T. M. & Bjornson, K. P. (1996). Mechanisms of helicase-catalyzed DNA unwinding. *Annu. Rev. Biochem.* **65**, 169–214.
47. Jose, D., Datta, K., Johnson, N. P. & von Hippel, P. H. (2009). Spectroscopic studies of position-specific DNA breathing fluctuations at replication forks and primer–template junctions. *Proc. Natl Acad. Sci. USA*, **106**, 4231–4236.
48. von Hippel, P. H. & Delagoutte, E. (2001). A general model for nucleic acid helicases and their "coupling" within macromolecular machines. *Cell*, **104**, 177–190.
49. Wang, H., Peskin, C. S. & Elston, T. C. (2003). A robust numerical algorithm for studying biomolecular transport processes. *J. Theor. Biol.* **221**, 491–511.
50. Wang, H. (2007). A new derivation of the randomness parameter. *J. Math. Phys.* **48**, 103301–103318.
51. Bortz, A. B., Kalos, M. H. & Lebowitz, J. L. (1975). A new algorithm for Monte Carlo simulation of Ising spin systems. *J. Comput. Phys.* **17**, 10–18.
52. Gillespie, D. T. (1977). Exact stochastic simulation of coupled chemical reactions. *J. Phys. Chem.* **81**, 2340–2361.
53. Zuker, M. (2003). Mfold web server for nucleic acid folding and hybridization prediction. *Nucleic Acids Res.* **31**, 3406–3415.
54. Santalucia, J. (1998). A unified view of polymer, dumbbell, and oligonucleotide DNA nearest-neighbor thermodynamics. *Proc. Natl Acad. Sci. USA*, **95**, 1460–1465.
55. Xia, T., SantaLucia, J., Burkard, M. E., Kierzek, R., Schroeder, S. J., Jiao, X. *et al.* (1998). Thermodynamic parameters for an expanded nearest-neighbor model for formation of RNA duplexes with Watson–Crick base pairs. *Biochemistry*, **37**, 14719–14735.
56. Ramstein, J. & Lavery, R. (1988). Energetic coupling between DNA bending and base pair opening. *Proc. Natl Acad. Sci. USA*, **85**, 7231–7235.
57. Johnson, D. S., Bai, L., Smith, B. Y., Patel, S. S. & Wang, M. D. (2007). Single-molecule studies reveal dynamics of DNA unwinding by the ring-shaped T7 helicase. *Cell*, **129**, 1299–1309.
58. Tomko, E. J., Fischer, C. J., Niedziela-Majka, A. & Lohman, T. M. (2007). A nonuniform stepping mechanism for *E. coli* UvrD monomer translocation along single-stranded DNA. *Mol. Cell*, **26**, 335–347.